Clinical Proteomics

RESEARCH

Open Access

Comprehensive analysis of proteomics and lactylation proteomics in ovarian granulosa cells of patients with polycystic ovary syndrome

Li Liu[1†], Qian Gao[2†], Jingyu Huang[1†], Yu Qian[1], Kailu Liu[1], Yun Tong[1], Yaqiong Zeng[1], Yueyi Li[1], Yunteng Liang[1], Yanli Hong[1*], Huifang Zhou[1*] and Xiaowei Nie[1*]

Abstract

Background Polycystic ovary syndrome (PCOS) is a complex and heterogeneous metabolic disorder that affects 6–20% of women of reproductive age. However, research on the lactylation-modified proteome in PCOS remains limited.

Methods This study included 30 patients with PCOS and 30 control subjects, all of whom underwent intracytoplasmic sperm injection or in vitro fertilization-embryo transfer treatments at the fertility center between October 2022 and May 2023. A 4-dimensional label-free proteomic quantitation method was applied to analyze enzymatically digested peptide fragments of granulosa cell proteins. Liquid chromatography–mass spectrometry was used for protein identification and quantification.

Results Bioinformatics analysis of differentially expressed proteins (DEPs) and differentially lactylated proteins identified 1057 DEPs between the two groups. Among these, 478 proteins were upregulated, and 579 were downregulated in the PCOS group. Regarding lactylation modifications, 668 proteins exhibited increased lactylation levels, while 1059 proteins indicated decreased lactylation levels in the PCOS group. Additionally, site-level analysis revealed 1041 upregulated and 2143 downregulated lactylation sites in the PCOS group.

Conclusions This study provides a comprehensive quantitative overview of proteomic and lactylation-modified proteomic expression profiles in granulosa cells from patients with PCOS, offering novel insights into PCOS research. Further research is needed to clarify the specific roles of protein lactylation in PCOS pathogenesis.

†Li Liu, Qian Gao, and Jingyu Huang have contributed equally to this work.

*Correspondence:
Yanli Hong
15951711586@126.com
Huifang Zhou
yfy0005@njucm.edu.cn
Xiaowei Nie
fsyy00636@njucm.edu.cn

Full list of author information is available at the end of the article

Keywords Polycystic ovary syndrome, Granulosa cells, Novel posttranslational modification, Bioinformatics analysis

Background

Polycystic ovary syndrome (PCOS) is a complex and heterogeneous metabolic condition characterized by persistent anovulation, hyperandrogenism, polycystic ovarian morphology, and progressive metabolic dysfunction [1]. The symptoms of PCOS often worsen with advancing age. Globally, PCOS affects an estimated 10% of women of reproductive age [2] and accounts for 70–80% of infertility cases related to anovulatory dysfunction [3]. Beyond reproductive challenges, women with PCOS face an increased risk of pregnancy-related complications and comorbidities, including type 2 diabetes mellitus, hypertension-related disorders, cardiovascular diseases, mental health conditions (depression and anxiety), and certain malignancies [4–6]. These conditions impose pronounced burdens not only on affected women and their families but also on societal healthcare resources. Although the molecular and endocrine mechanisms underlying PCOS remain incompletely understood, they are believed to involve a complex interplay of genetic predisposition, environmental factors [1], and epigenetic regulation [7].

Posttranslational protein modifications play a crucial role in regulating diverse pathological and physiological processes. In PCOS, several posttranslational modifications have been verified, including phosphorylation, methylation, acetylation, ubiquitination, and crotonylation [8, 9]. Lactylation, a recently discovered posttranslational modification, specifically targets lysine residues on proteins. By regulating protein activity and function, lactylation influences gene expression and intercellular communication [10]. Emerging evidence highlights lactylation as a crucial regulatory mechanism in a wide range of physiological and pathological processes, including cancer, inflammation, immune responses, tumor microenvironments, neurodegenerative diseases, metabolic disorders, and cardiovascular diseases [6, 11–13]. With recent advances in proteomic technologies, researchers have increasingly focused on the role of posttranslational lactylation in disease pathogenesis. Prior studies have demonstrated that exogenous lactate supplementation improves oocyte maturation and enhances embryonic developmental potential, suggesting a potential regulatory role of lactylation in these processes [14]. Wu et al. [15] further reported that hypoxia accelerates (hCG)-induced granulosa cells (GCs) luteinization by stimulating lactate production and lactylation, thereby identifying lactylation as a new modulator of GC luteinization. In patients with PCOS, lactate levels in follicular fluid and GCs are significantly reduced [16, 17], accompanied by marked downregulation of lactate dehydrogenase A (LDHA) expression in GCs [18]. Since follicle development in patients with PCOS requires higher lactate levels for appropriate stimulation [19], impaired lactate production in GCs—potentially mediated by dysregulation of the NAMPT/SIRT2/LDHA pathway—has been implicated in defective follicle development [20]. Collectively, these findings underscore the central role of reduced lactate availability in the progression of PCOS. Nevertheless, studies investigating the lactylation-modified proteome in GCs of patients with PCOS remain scarce.

This study aims to investigate the potential impact of posttranslational lactylation on ovarian metabolic homeostasis and oocyte developmental potential in patients with PCOS compared to control subjects. Using 4-dimensional (4D) label-free proteomics quantification technology, a quantitative analysis of protein and lactylation site differences was conducted between PCOS and control groups. Bioinformatics methods were employed to identify differentially expressed proteins (DEPs) and potential lactylation sites associated with PCOS development, thereby elucidating their roles in PCOS pathogenesis.

Methods

Population

A total of 60 participants were enrolled, including 30 patients with PCOS and 30 control subjects with tubal or male factor infertility who underwent in vitro fertilization (IVF). All participants were recruited from the Reproductive Medicine Center of Jiangsu Province Hospital of Chinese Medicine between October 2022 and May 2023. PCOS diagnosis was established according to the 2003 Rotterdam Consensus criteria [21]. The study protocol was reviewed and approved by the Ethics Committee of Jiangsu Province Hospital of Chinese Medicine (Approval No. 2022NL-200-03). Written informed consent was achieved from all participants.

Collection of GCs

A standardized mid-luteal long protocol was administered to all patients utilizing a gonadotropin-releasing hormone agonist. Ovulation was induced through the administration of 10,000 IU hCG on the scheduled day. On the day of oocyte retrieval, follicular fluid of mature follicles (>14 mm) was pooled and centrifuged at 2000×*g* for 10 min. The pellet was resuspended and incubated with 0.1% hyaluronidase (Sigma, USA) at 37 °C for 20 min, followed by the addition of Ficoll–Paque (GE Healthcare, Sweden) for density gradient centrifugation at 600×*g* for 10 min. Purified GCs were collected from the interlayer phase and stored at −80 °C until use.

Transmission electron microscopy (TEM)

GCs derived from patients with PCOS were fixed using 2.5% glutaraldehyde (Sigma-Aldrich, St. Louis, MO, USA) for 48 h. After fixation, GCs underwent dehydration utilizing a graded ethanol series. The samples were subsequently prepared for observation through TEM (Thermo Fisher Scientific, Hillsboro, OR, USA).

Detection of the lactylated proteome

The GC samples were lysed employing sonication in ice-cold buffer containing 1% SDS, 1% protease inhibitor cocktail, 3 μM trichostatin A, and 50 mM nicotinamide. Cellular debris was removed by centrifugation (12,000×*g*, 10 min, 4 °C), and the supernatant was collected for protein quantification through bicinchoninic acid assay. Protein precipitation was conducted through pre-cooled acetone (−20 °C, 2 h), followed by two washing cycles and final re-suspension in 200 mM triethylammonium bicarbonate. Proteins were minimized using 5 mM dithiothreitol (56 °C, 30 min) and subsequently alkylated with 11 mM iodoacetamide under denaturing conditions (in the dark, 15 min). Trypsin digestion was performed overnight at 37 °C at a 1:50 (w/w) enzyme-to-protein ratio. Peptide purification was conducted using Strata™-X SPE columns (Phenomenex, Torrance, CA, USA). For lactylation enrichment, peptides were dissolved in NETN buffer (100 mM NaCl, 1 mM EDTA, 50 mM Tris–HCl, 0.5% NP-40, pH 8.0) and incubated overnight at 4 °C with anti-pan-lactylation antibody-conjugated beads (PTM Biolabs, Hangzhou, China). After sequential washing with NETN buffer and deionized water, bound peptides were eluted with 0.1% trifluoroacetic acid, lyophilized, and desalted using C_{18} ZipTips (MilliporeSigma, Burlington, MA, USA).

Liquid chromatography–mass spectrometry (LC–MS) analysis was supported by Jingjie PTM BioLabs (Hangzhou, China). Briefly, tryptic peptides were dissolved in solvent A (0.1% formic acid, 2% acetonitrile in water) and separated on a homemade reversed-phase analytical column (25 cm length, 100 μm i.d.) using a nanoElute UHPLC system (Bruker Daltonics). Following being subjected to a capillary source, the peptides were subjected to timsTOF Pro (Bruker Daltonics) MS for further analysis in parallel accumulation serial fragmentation mode. MS data were processed by the MaxQuant search engine software (version 1.6.6.0). Tandem mass spectra were searched employing the human SwissProt database (20,366 entries) and the reverse decoy database. FDR < 1%. The relative quantitative values of modified peptides in various samples were obtained by centralizing the signal intensity values in different samples. Following the filtering of lysine lactylation sites (localization probability > 0.75), the relative quantitative values of each sample were obtained from two experiments. Quantification of Lactylation Proteins: The relative quantification value of each modification site was divided by that of the corresponding protein to account for differences in protein expression. Statistical analysis of DEPs and differentially lactylated proteins (DLPs): The ratio of relative quantification values of proteins and modification sites between the two samples was considered as fold change (FC). A key upregulation threshold is set as a change reaching 1.5, and a significant downregulation threshold as a change below 1/1.5.

Functional gene ontology (GO) and Kyoto encyclopedia of genes and genomes (KEGG) pathway enrichment analyses

GO and KEGG enrichment analyses were conducted using the R package "clusterProfiler".

Protein annotations obtained from the GO framework are classified into three functional categories: Biological process, cellular component, and molecular function. To examine significantly enriched GO terms among differentially modified proteins, we performed GO enrichment analysis employing Fisher's exact test, with those verified in the dataset acting as the background. Terms with a $P < 0.05$ were deemed statistically significant.

For pathway enrichment analysis of differentially modified proteins, we used the KEGG database. Similarly, Fisher's exact test was used to assess the statistical significance of pathway enrichment, with those identified in the dataset serving as the background. Pathways with a $P < 0.05$ were considered significant.

Protein–protein interaction (PPI) network and hub protein analyses

PPI networks were constructed using the open-access online protein–protein interaction analysis tool STRING (https://cn.string-db.org/). DEPs and DLPs were screened, exceeding a threshold of 1.5-FC, and subsequently imported into the STRING database to assess PPI networks. Protein interaction correlations were extracted employing a confidence score > 0.7 (high confidence). Visualization of the differential interaction network was conducted using the R package "visNetwork". The visual network diagram for hub protein screening was generated employing Cytoscape (http://www.cytoscape.org/). Hub protein screening was conducted using the CytoHubba (https://apps.cytoscape.org/apps/cytohubba) and MCODE (https://apps.cytoscape.org/apps/mcode) plugins within Cytoscape.

Statistical analysis

Statistical analyses were conducted using GraphPad Prism software (version 10.1.2). The data were assessed for normality and homogeneity of variance. Independent *t* tests were employed for between-group comparisons.

Data are expressed as mean ± standard deviation (SD). Statistical significance was set at a threshold of $P < 0.05$.

Results

Clinical characteristics of participants

Clinical and assisted reproductive technology outcomes were compared between PCOS and control participants (Table 1). Non-significant differences were observed in the following parameters: Age, height, weight, body mass index (BMI), luteinizing hormone (LH), estradiol (E2), progesterone (P), prolactin (PRL), total gonadotropin (GN) dosage, nuclear maturation (MII) rate, 2-pronuclear (2PN) fertilization rate, number of transferable embryos, and high-quality embryo rate ($P > 0.05$). Conversely, significantly higher values were observed in patients with PCOS for anti-Müllerian hormone (AMH), LH/FSH ratio, total testosterone (TT), antral follicle count (AFC; bilateral ovaries), GN duration, oocytes retrieved, mature (MII) oocytes, cleavage-stage embryos, total embryos, and blastocyst count ($P < 0.05$). These results are aligned with the metabolic and hormonal dysregulation characteristic of PCOS, especially the phenotypes of hyperandrogenism and ovarian hyperstimulation.

Table 1 Demographic and Clinical Characteristics of Patients with PCOS and CON

Parameter	CON ($N = 30$)	PCOS ($N = 30$)	*P* value
Age (year)	30.47 ± 3.1	29.97 ± 3.93	0.584
Height (cm)	1.62 ± 0.05	1.64 ± 0.05	0.375
Weight (kg)	62.48 ± 11.6	65.1 ± 10.25	0.355
BMI (kg/m^2)	23.57 ± 3.61	24.3 ± 3.55	0.431
AMH (ng/ml)	4.75 ± 4.38	9.09 ± 5.11	<0.001
FSH (IU/L)	7.27 ± 1.59	6.45 ± 1.3	0.031
LH (IU/L)	5.18 ± 7.99	6.43 ± 3.02	0.428
LH/FSH	0.64 ± 0.66	1.03 ± 0.54	0.017
E2 (pg/ml)	46.79 ± 25.41	41.59 ± 21.15	0.398
TT (ng/ml)	36.55 ± 15.03	46.68 ± 17.8	0.020
P (ng/ml)	0.61 ± 0.29	0.46 ± 0.38	0.256
PRL (ng/ml)	18.17 ± 11.68	14.57 ± 8.46	0.282
Left AFC	8.53 ± 2.22	11.03 ± 1.71	<0.001
Right AFC	9.2 ± 2.7	11.07 ± 1.57	0.001
Gonadotropin dosage (IU)	2182.5 ± 469.28	2133.58 ± 542.29	0.709
GN duration (day)	9.57 ± 1.65	10.53 ± 1.55	0.022
No. of oocytes retrieved	12.47 ± 6.17	16.67 ± 6.41	0.011
No. of MII oocytes	10.4 ± 6.24	13.87 ± 5.38	0.024
Nuclear maturation (MII) rate	0.82 ± 0.18	0.85 ± 0.15	0.497
2PN	7.7 ± 4.89	10.87 ± 5.63	0.023
2PN fertilization rate	0.59 ± 0.17	0.64 ± 0.19	0.246
No. of cleavage-stage embryos	9.43 ± 5.7	13.14 ± 7.07	0.031
Total embryo count	7.63 ± 5.07	10.43 ± 5.58	0.047
No. of transferable embryos	4.23 ± 2.86	5.63 ± 3.36	0.088
High-quality embryo	4.73 ± 4.39	6.17 ± 3.81	0.181
High-quality embryo rate	0.61 ± 0.86	0.59 ± 0.68	0.831
Blastocyst count	2.37 ± 2.63	4.4 ± 3.92	0.021

CON normal ovarian reserve function, *PCOS* polycystic ovary syndrome, *BMI* body mass index, *AMH* anti-Müllerian hormone, *FSH* follicle-stimulating hormone, *LH* luteinizing hormone, *E2* estradiol, *TT* total testosterone, *P* progesterone, *PRL* prolactin, *AFC* antral follicle count, *GN* gonadotropin, *MII* metaphase II, *2PN* 2-pronuclear

Group comparisons utilized the unpaired *t* test for statistical evaluation; $P < 0.05$ is in bold. A $P < 0.05$ indicates statistical significance was identified between different groups. Data are presented as mean ± SD

TEM observation of ultrastructural alterations in GCs of patients with PCOS

To investigate the changes in mitochondrial ultrastructure in GCs from patients with PCOS, we conducted TEM analysis (Fig. 1). The findings revealed significant mitochondrial damage, such as outer mitochondrial membrane disruption (extensive dissolution) and structural disorganization of mitochondrial cristae in GCs from patients with PCOS.

Proteomics analysis

A total of 6393 proteins and 56,935 peptides were detected in proteomics (Supplementary Table S1), and 1057 DEPs were found, comprising 478 upregulated and 579 downregulated proteins in the PCOS group (Fig. 2A). The top 10 upregulated and downregulated proteins are presented in Fig. 2B, with 10 proteins in each category. Subcellular localization annotation revealed that most DEPs were distributed across the following compartments: Nucleus (33.77%), cytoplasm (19.58%), extracellular space (16.65%), mitochondria (12.3%), and plasma membrane (11.45%) (Fig. 2C). The complete list of DEPs is available in Supplementary Table S2.

Functional classification of DEPs

The functional enrichment patterns of DEPs between the two groups were analyzed using GO enrichment analysis and KEGG pathway analysis. The findings revealed that DEPs were significantly enriched in several biological processes, including blood coagulation, fibrin clot formation, keratinocyte differentiation, and the positive regulation of interleukin-8 production (Fig. 3A). In terms of cellular components, DEPs were significantly localized in keratin filaments, cornified envelope, the extracellular space, intermediate filaments, and the intermediate filament cytoskeleton (Fig. 3B). Additionally, DEPs displayed functional enrichment in molecular functions, including structural constituent of skin epidermis, MHC class II receptor activity, MHC class II protein binding, choline binding, lipopeptide binding, and other molecular functions (Fig. 3C). Additionally, KEGG pathway enrichment analysis indicated that DEPs were enriched in several crucial biological processes, including the complement and

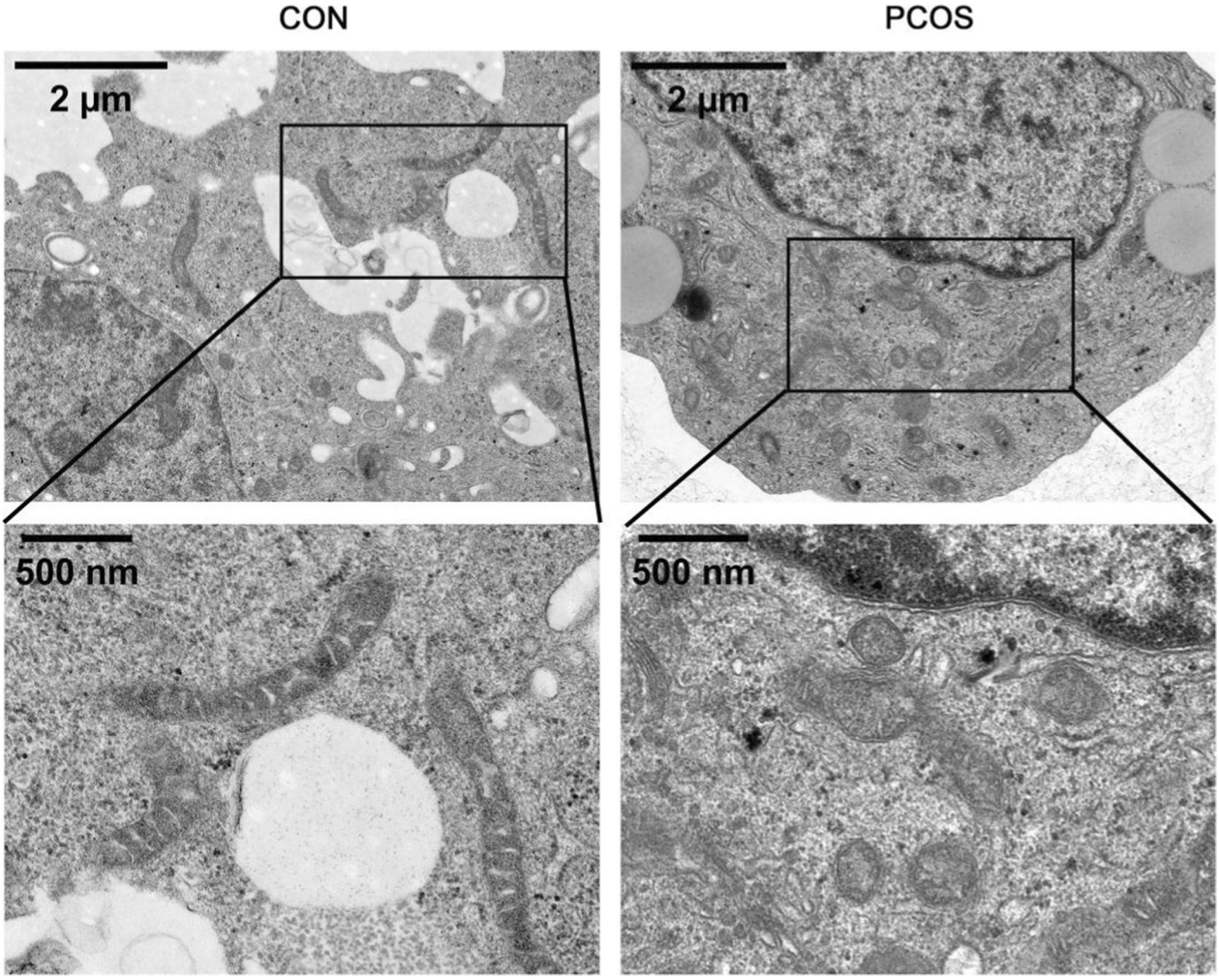

Fig. 1 GCs from patients with PCOS were examined using TEM. Scale bars: 1 μm (overview), 500 nm (inset)

coagulation cascades, staphylococcus aureus infection, osteoclast differentiation, intestinal immune network for IgA production, the NOD-like receptor signaling pathway, and RIG-I-like receptor signaling pathway (Fig. 3D).

PPI network analysis of DEPs

Following filtering of DEPs data (FC ≥ 1.5), PPI networks were constructed employing the STRING database software (version 11.0). Interactions were extracted based on a confidence score exceeding 0.7 (high confidence). In the PPI network of DEPs, 1035 nodes and 1363 edges were identified. In the visualization, circles represent differential proteins, with color differentiation indicating their expression status: Blue for downregulated proteins and red for upregulated proteins. The intensity of the color reflects the magnitude of the FC, while the size of each circle corresponds to the number of interacting proteins. The top 50 proteins with the highest number of interactions were used to construct the PPI network (Fig. 4), revealing that these interactions were predominantly enriched in processes related to thrombosis, anticoagulation, and the negative regulation of fibrinolysis.

Lactylation proteomics analysis and functional classification of DLPs

To comprehensively analyze lactylation modifications in PCOS, GCs were collected from 30 patients with PCOS and 30 healthy controls (undergoing IVF treatment) and divided into two groups for quantitative proteomic analysis by LC–MS. Conversely, 1949 proteins and 5497 modified peptides were identified in lactylation proteomics (Supplementary Table S3). A total of 3184 lactylation sites were identified across 1727 proteins, with a FC threshold of >1.5 between groups. Specifically, 1041 sites on 668 proteins displayed increased lactylation in PCOS, while 2143 sites on 1059 proteins indicated decreased lactylation (Fig. 5A). Detailed information on all DLPs is provided in Supplementary Table S4. Proteins were grouped based on FC into four categories: Q1 (0–0.5), Q2 (0.5–0.67), Q3 (1.5–2), and Q4 (>2; Fig. 5B). Subsequent

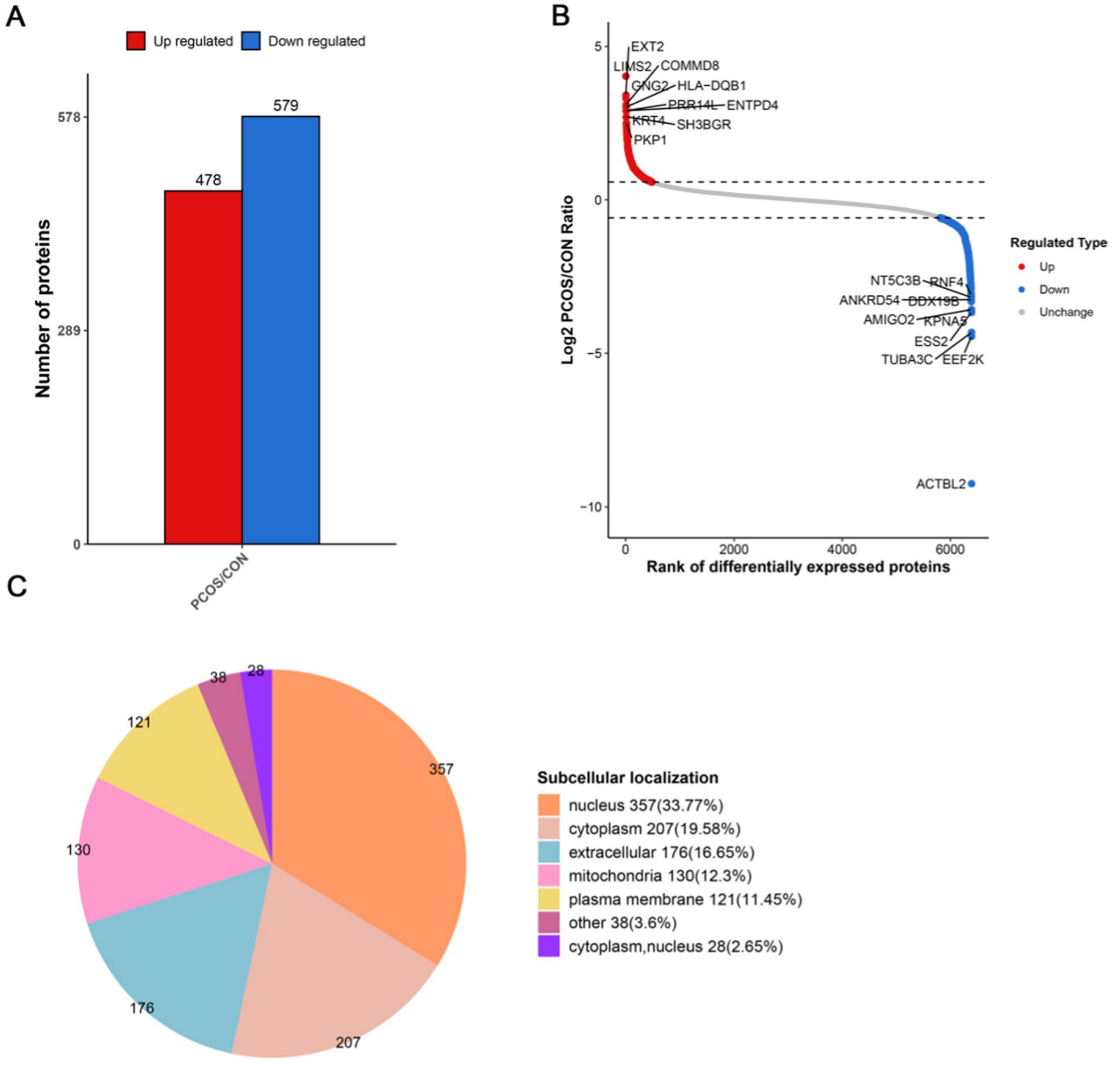

Fig. 2 Quantitative analysis of DEPs in GCs from control and PCOS women. **A** Identification of DEPs. **B** Scatter plot depicting protein distribution, where the *x*-axis represents ranked FC values (ratio) from highest to lowest, and the *y*-axis represents $\log_2$-transformed FC values. Red dots indicate significantly upregulated proteins, blue dots indicate significantly downregulated proteins, and gray dots represent proteins with non-significant differences. **C** Subcellular localization of DEPs is depicted below

bioinformatics analyses were conducted to evaluate these DLPs. Lactylated proteins were significantly distributed in the nucleus (43.3%), cytoplasm (32.19%), mitochondria (7.4%), and extracellular space (6.01%; Fig. 5C).

DLPs were significantly enriched in different biological processes, including the positive regulation of type I interferon production, positive regulation of the centrosome cycle, pore complex assembly, neural crest cell migration, and bicarbonate transport (Fig. 5D). Besides, DLPs were predominantly enriched in specific cellular components, including specific granule lumen, receptor complex, Sin3-type complex, and Sin3 complex (Fig. 5E), underscoring the role of lactylation in cellular organelle function, signal transduction, and gene regulation. At the molecular function level, DLPs were primarily enriched in R-SMAD binding and beta-catenin binding (Fig. 5F). The KEGG pathway enrichment analysis demonstrated that these proteins were primarily correlated with pathways, including Staphylococcus aureus infection, cell adhesion molecules, Th17 cell differentiation, and inflammatory bowel disease signaling (Fig. 5G). Hierarchical cluster analysis of proteins in Q1–Q4 groups indicated

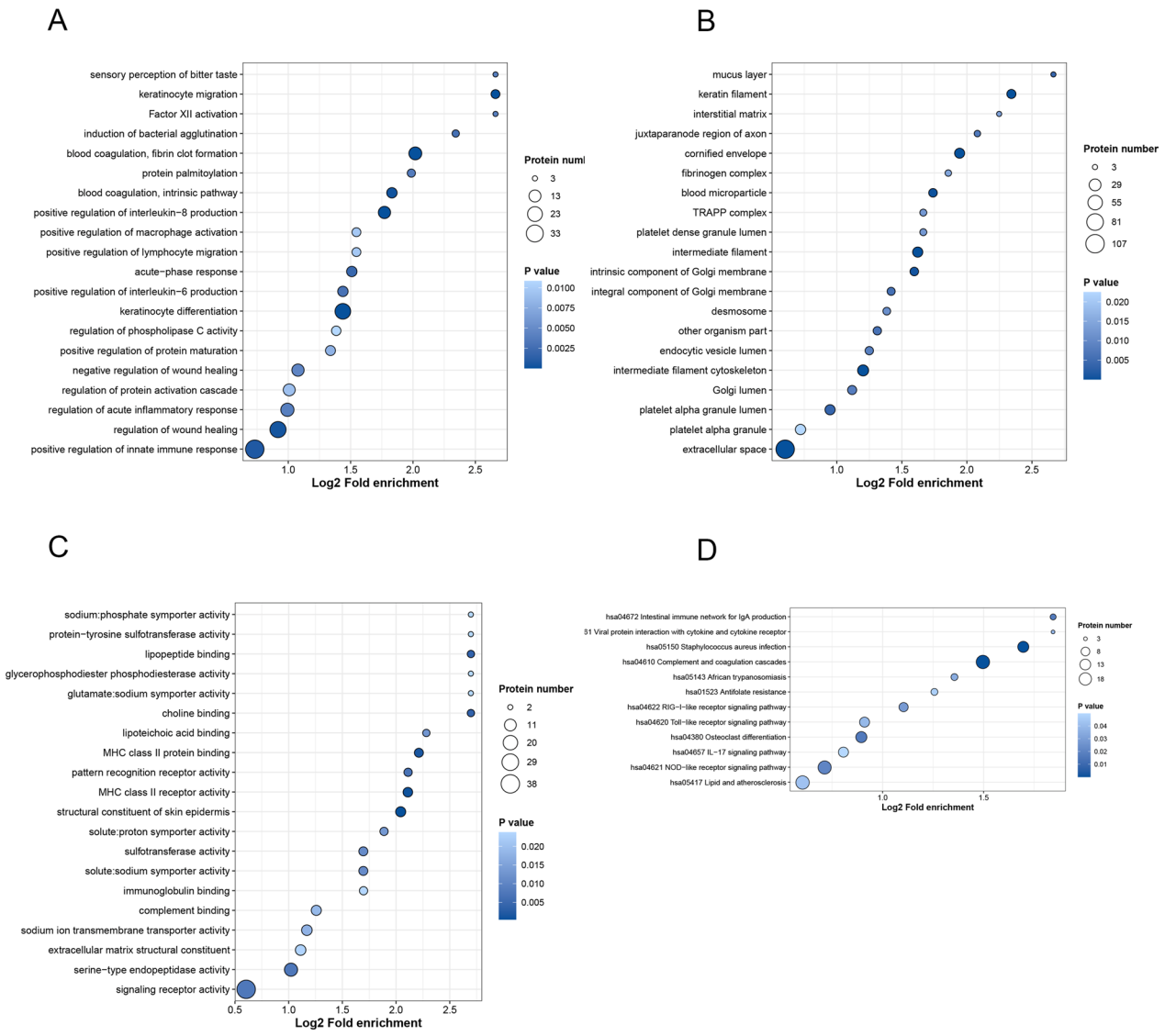

Fig. 3 Integrated Bioinformatics Analysis of DEPs. GO annotations are hierarchically classified into three categories: **A** biological process, **B** cellular component, and **C** molecular function, respectively. **D** The KEGG pathway enrichment analysis is conducted for DEPs

that mRNA metabolic processes, RNA processing, RNA splicing, and negative regulation of gene expression were associated with Q1 and Q2 groups (characterized by the lower lactylation levels; Fig. 5H), highlighting the role of lactylation in post-transcriptional regulation. These results indicate widespread dysregulation of protein lactylation modifications in PCOS.

PPI network analysis of DLPs and hub proteins identification

After filtering the DLPs dataset using an FC threshold of 1.5, interactions for DLPs were extracted from the STRING database software (version 11.0) based on a confidence score > 0.7 (high confidence). As illustrated in Fig. 6A, circles represent differentially modified proteins, with various colors indicating the protein's differential expression status: Blue for downregulated modified proteins, red for upregulated modified proteins, and yellow for proteins containing both upregulated and downregulated modification sites. The size of each circle corresponds to the number of interacting proteins. To construct the protein interaction network (Fig. 6A), the top 50 proteins with the highest number of interactions were selected, demonstrating that DLPs cluster within the R-SMAD pathway.

Based on molecular function enrichment analysis and PPI results, DLPs linked with the R-SMAD pathway were identified (Table 2). Utilizing the STRING database and CytoHubba algorithm, hub protein analysis was performed on the proteins listed in Table 2, identifying the top five hub proteins with the highest connectivity (Fig. 6B). These proteins exhibit strong connectivity

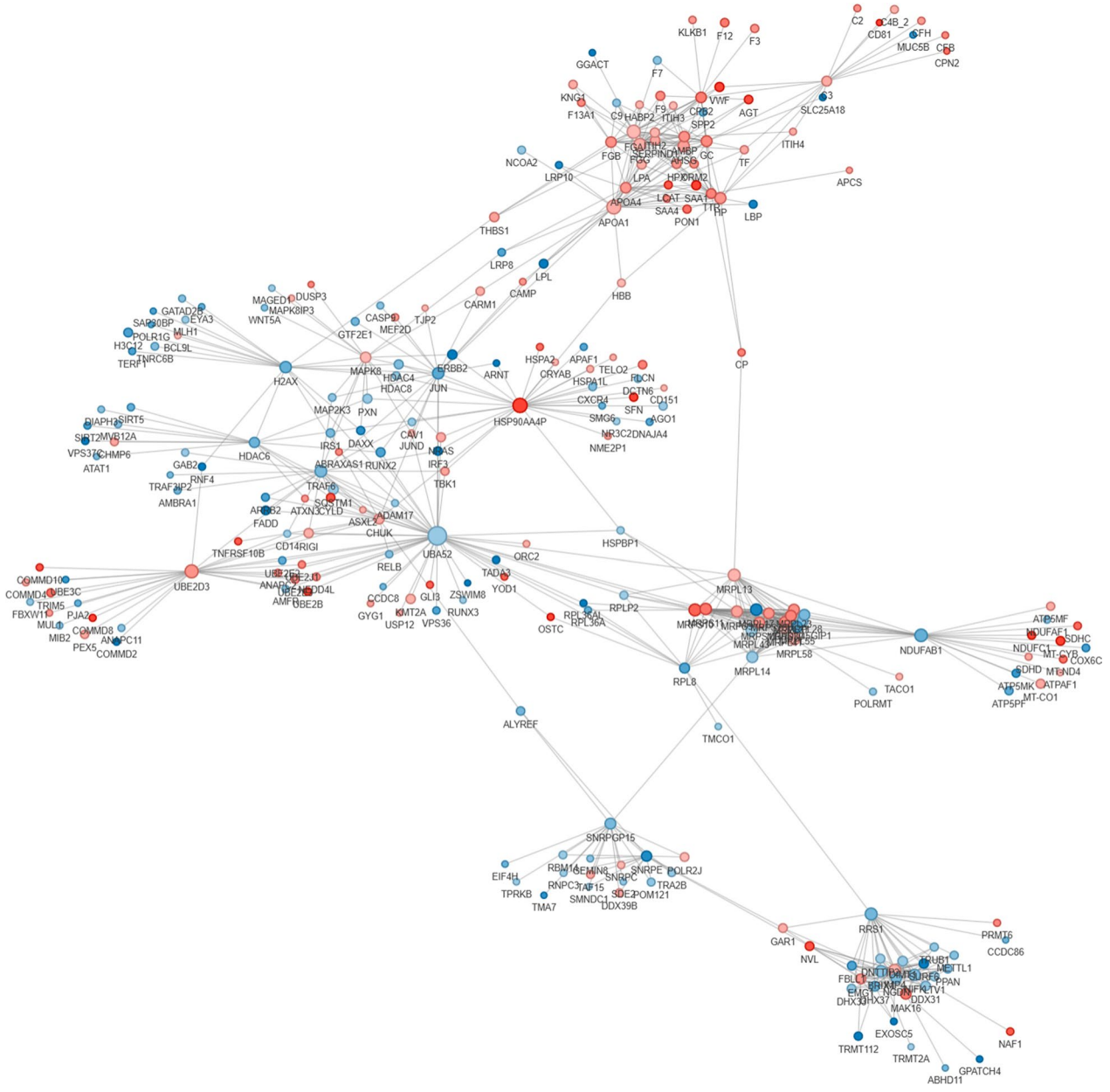

Fig. 4 Analysis of PPI Network in DEPs. The figure illustrates a PPI network where circles represent DEPs, with color coding indicating their differential expression. Red represents downregulated proteins, while blue indicates upregulated proteins. DEPs are proteins that are differentially expressed, and PPI refers to interactions between proteins

and may serve as major regulatory factors or key effectors in the molecular mechanisms underlying PCOS. Subsequently, a comprehensive clustering analysis of the PPI network was conducted using the MCODE algorithm to identify crucial functional modules. This analysis yielded a network comprising mothers against decapentaplegic homolog 2 (SMAD2), SMAD3, poly [ADP-ribose] polymerase 1, catenin beta-1 (CTNNB1), histone acetyltransferase (HAT) p300 (EP300), transcription factor Jun (JUN), transcriptional repressor protein YY1, zinc finger E-box-binding homeobox 2, and SNW domain-containing protein 1 (Fig. 6C).

Notably, SMAD3, SMAD2, CTNNB1, EP300, and JUN were found as potential hub proteins by the Cyto-Hubba algorithm and validated through MCODE clustering analysis, verifying their crucial roles in the R-SMAD pathway.

Integrated analysis of proteomics and lactylation-omics

Based on the $\log_2$ FC values and the defined thresholds obtained from proteomics and lactoylome data,

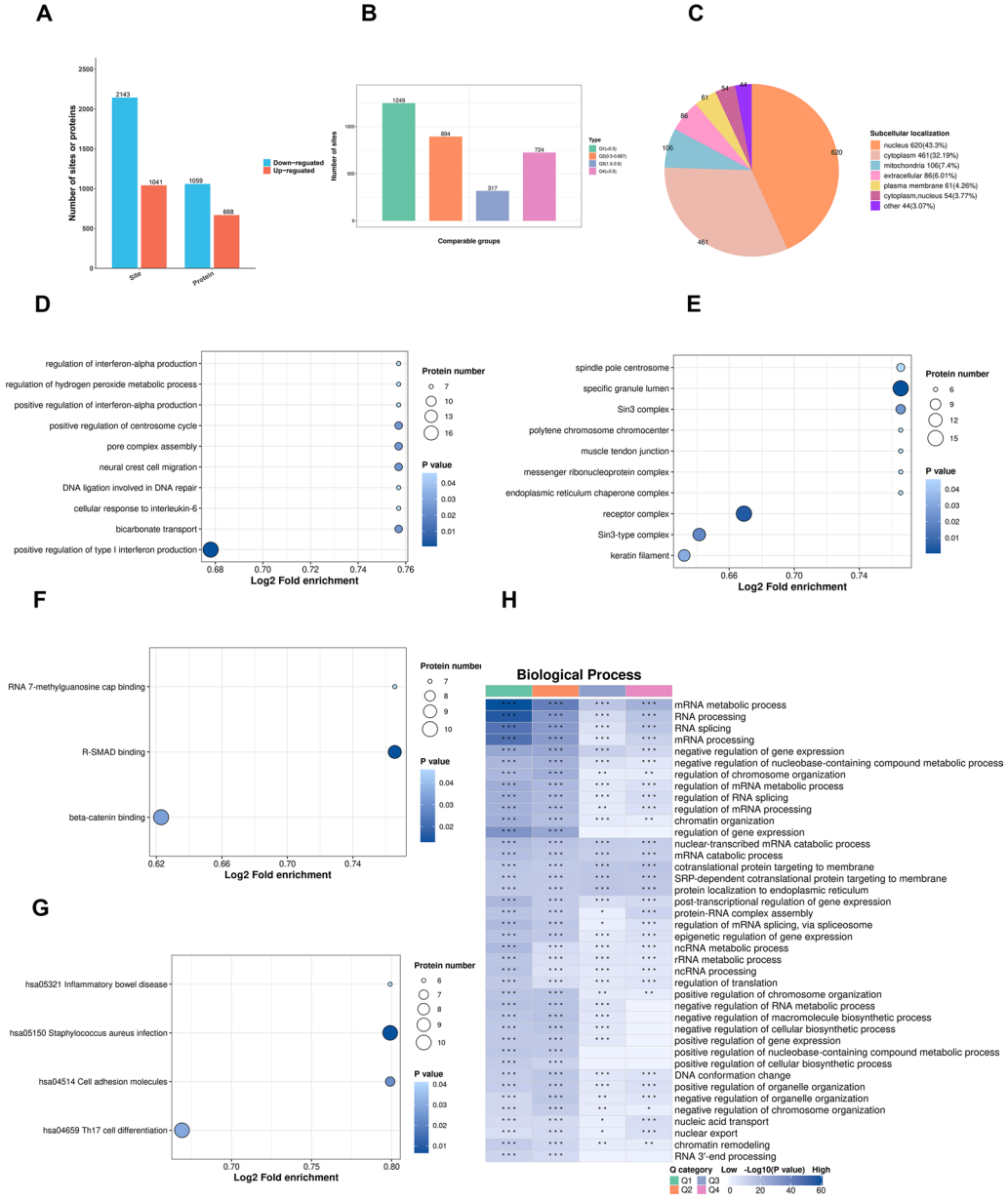

Fig. 5 Comprehensive profiling of lactylation-modified protein residues in PCOS. **A** Differential lysine lactylation sites (FC thresholds > 1.5) and associated proteins found in PCOS versus control cohorts. **B** Stratification of lactylated proteins into four subsets based on differential expression thresholds: Q1 (0–0.5), Q2 (0.5–0.67), Q3 (1.5–2), and Q4 (>2). **C** Subcellular localization of lactylation-modified proteins, demonstrating compartment-specific enrichment patterns. GO enrichment analysis of lactylated proteins across biological processes (**D**), cellular components (**E**), and molecular functions (**F**). **G** KEGG pathway enrichment analysis highlighting dysregulated metabolic and signaling pathways. **H** Hierarchical clustering of GO biological processes across Q1–Q4 groups, demonstrating functional divergence in lactylation dynamics. Data were analyzed employing Fisher's exact test, with significance thresholds defined as $P < 0.05$

statistical analyses were performed to assess the distributions of DEPs across both omics datasets. The findings were visualized in a nine-quadrant plot (Fig. 7A). Subsequently, proteins were categorized into nine distinct groups according to their thresholds at both the protein level and lactoylation levels. Biological process enrichment analyses were then performed for proteins within each category (Fig. 7B). When protein levels remained unchanged while lactoylation levels decreased, the enriched biological processes were significantly related to the negative regulation of DNA metabolic processes. Conversely, when protein levels remained unchanged but lactylation levels increased, the enriched processes were primarily associated with the positive regulation of protein localization, control of protein import, regulation of intracellular protein transport, and protein import into

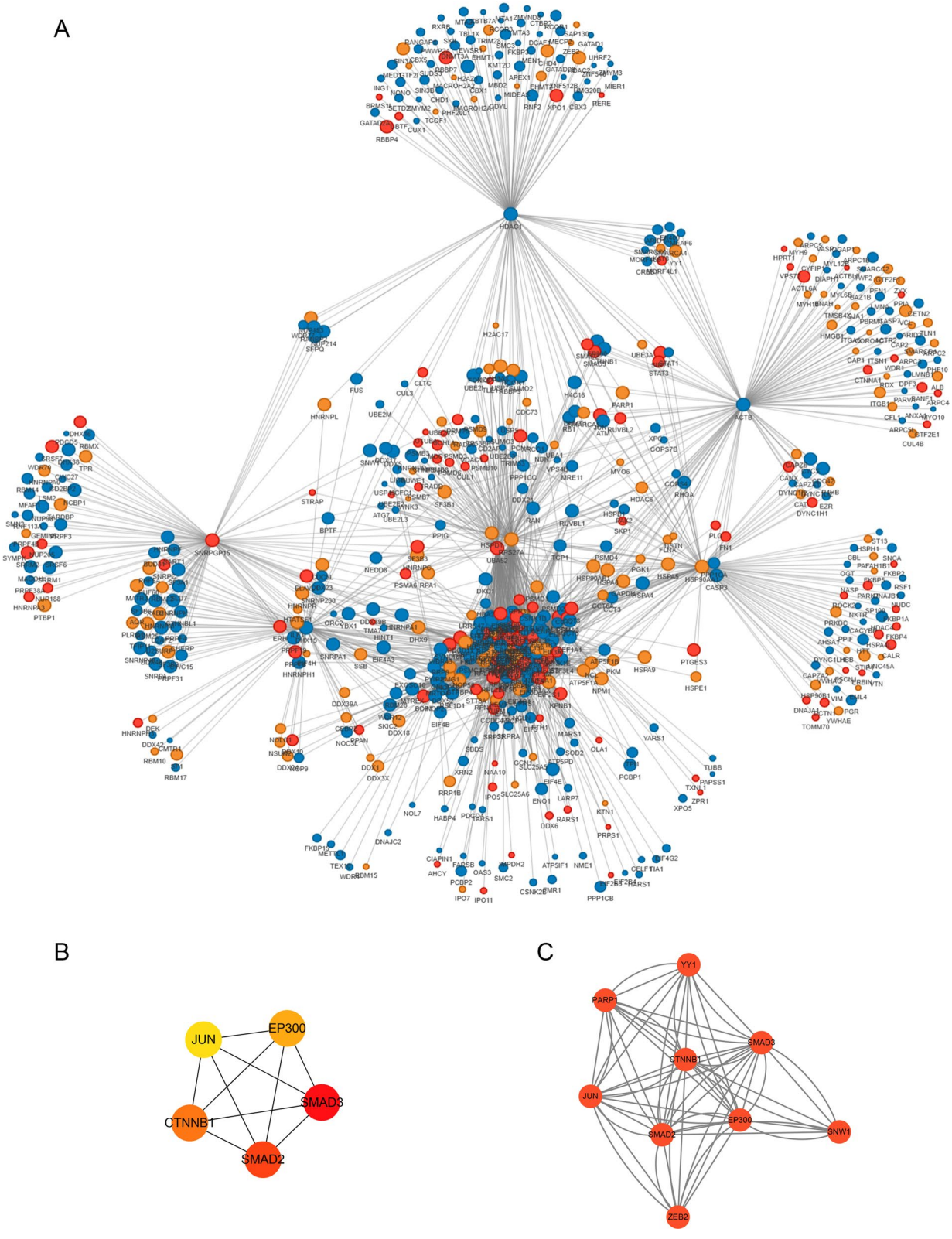

Fig. 6 PPI Analysis of DLPs. **A** PPI network of DLPs is depicted, with circular nodes representing DLPs. Different colors indicate the differential expression of proteins: red represents downregulated lactated proteins, while blue signifies upregulated lactated proteins. **B** The top five key DLPs associated with R-SMAD were identified using CytoHubba, and a network was constructed. Nodes represent proteins, while edges indicate physical interactions or functional correlations between proteins. Color intensity increases with protein ranking. **C** A cluster module of DLPs associated with R-SMAD was identified using the MCODE algorithm

Table 2 DLPs associated with R-SMAD

Protein accession	Position	Amino acid	Gene name	PCOS/CON ratio	Regulated type
Q15796	157	K	SMAD2	8.908738255	Up
P09874	254	K	PARP1	8.42777358	Up
P84022	117	K	SMAD3	8.085499786	Up
P21333	2387	K	FLNA	4.123654312	Up
P21333	2515	K	FLNA	3.926948937	Up
P21333	626	K	FLNA	3.277851197	Up
P21333	578	K	FLNA	2.572832352	Up
P05412	268	K	JUN	2.272491904	Up
P21333	1372	K	FLNA	2.260247686	Up
P21333	2473	K	FLNA	2.226211081	Up
P21333	1593	K	FLNA	2.205118489	Up
P21333	58	K	FLNA	1.956357096	Up
O60315	1024	K	ZEB2	1.894014523	Up
O95373	119	K	IPO7	1.8704582	Up
P21333	771	K	FLNA	1.826706024	Up
P21333	92	K	FLNA	1.786448152	Up
P21333	508	K	FLNA	1.718512342	Up
P62942	35	K	FKBP1A	1.686541164	Up
O60315	993	K	ZEB2	1.660894282	Up
P25490	409	K	YY1	1.63635248	Up
P21333	1547	K	FLNA	0.652253456	Down
P09874	852	K	PARP1	0.644640269	Down
P21333	1071	K	FLNA	0.636906965	Down
P21333	2607	K	FLNA	0.636429101	Down
P17844	33	K	DDX5	0.627542298	Down
P21333	700	K	FLNA	0.627232607	Down
O60315	485	K	ZEB2	0.624818748	Down
P21333	2563	K	FLNA	0.620304252	Down
P09874	97	K	PARP1	0.610229194	Down
O60315	555	K	ZEB2	0.597637112	Down
P09874	498	K	PARP1	0.583915175	Down
O15397	17	K	IPO8	0.570181539	Down
P21333	876	K	FLNA	0.563430496	Down
P21333	1007	K	FLNA	0.556495692	Down
P09874	654	K	PARP1	0.536537461	Down
P09874	105	K	PARP1	0.535999259	Down
P17844	32	K	DDX5	0.527309569	Down
P21333	2540	K	FLNA	0.51946595	Down
O60315	332	K	ZEB2	0.517921426	Down
P09874	518	K	PARP1	0.508046546	Down
P21333	2569	K	FLNA	0.498156523	Down
Q9UPN9	950	K	TRIM33	0.498067352	Down
Q13573	110	K	SNW1	0.491885481	Down
P25490	183	K	YY1	0.489440597	Down
P21333	1375	K	FLNA	0.462074915	Down
Q9H6Z4	165	K	RANBP3	0.458056432	Down
Q09472	14	K	EP300	0.450766119	Down
Q13573	170	K	SNW1	0.448556372	Down
O95373	1009	K	IPO7	0.444884316	Down
P21333	781	K	FLNA	0.434863826	Down
P21333	2215	K	FLNA	0.412811551	Down
P17844	490	K	DDX5	0.392665662	Down
P12757	45	K	SKIL	0.367143011	Down

Table 2 (continued)

Protein accession	Position	Amino acid	Gene name	PCOS/CON ratio	Regulated type
P09874	629	K	PARP1	0.366376307	Down
P21333	1801	K	FLNA	0.350464791	Down
O60315	762	K	ZEB2	0.348760836	Down
O00255	507	K	MEN1	0.346351661	Down
P25490	208	K	YY1	0.327339817	Down
P09874	633	K	PARP1	0.303468834	Down
P09874	221	K	PARP1	0.291828436	Down
Q09472	1569	K	EP300	0.137983812	Down
Q9H6Z4	145	K	RANBP3	0.137617433	Down
P35222	19	K	CTNNB1	0.036646969	Down

the nucleus. When protein levels decreased or remained unchanged while lactoylation levels also decreased or remained unchanged, the enriched processes were primarily linked to keratinocyte differentiation and the establishment of the skin barrier. Notably, when protein levels increased, lactylated proteins exhibited significant enrichment in biological processes, including the regulation of heterotypic cell–cell adhesion, blood coagulation, fibrin clot formation, negative regulation of wound healing, regulation of protein activation cascades, positive regulation of the MAPK cascade, induction of bacterial aggregation, as well as regulation of endothelial cell apoptosis.

Discussion

PCOS is a common heterogeneous condition characterized by reproductive and metabolic dysfunctions [22, 23]. GCs in patients with PCOS play a crucial role in supporting oocyte development and follicle maturation [24, 25]. In this research, 4D label-free proteomics technology was used to characterize the proteomic and lactylomic profiles of GCs in patients with PCOS. Initially, the dynamic alterations in lactoylation modification patterns in GCs of patients with PCOS were systematically characterized. A total of 1057 DEPs (478 upregulated and 579 downregulated) and 1727 DLPs (668 upregulated and 1059 downregulated) were identified in GCs of patients with PCOS. Moreover, these results underscore the importance of considering DEPs and DLPs in the investigation of PCOS pathogenesis.

Proteomics analysis indicated that DEPs were predominantly enriched in biological processes, including blood coagulation, fibrin clot formation, keratinocyte differentiation, and the positive regulation of interleukin-8. These results suggest that PCOS is closely correlated with abnormal protein expression patterns, especially in pathways linked with inflammation and immune responses. Notably, the key enrichment of DEPs in keratinocyte differentiation and skin barrier formation underscores the potential role of skin abnormalities in PCOS, which may be associated with the hyperandrogenism observed in patients with PCOS [26]. Furthermore, PPI network analysis demonstrated that DEPs were significantly concentrated in processes associated with thrombosis, anticoagulant therapy, and the negative regulation of fibrinolysis. These results imply that patients with PCOS may exhibit abnormalities in clotting functions, potentially contributing to the higher cardiovascular disease risk observed in this population, aligned with our previous findings [27].

Lactylation is a crucial posttranslational modification of proteins, regulating protein function, stability, and subcellular localization [10]. Although the role of lactylation in inflammation, immunity, and metabolic conditions has been widely studied, its involvement in ovarian function remains poorly understood. Lactylation has been implicated in different biological processes, especially playing a crucial role in oocyte maturation and embryonic development [14]. Hypoxic in vitro culture has been indicated to minimize histone lactylation and impair preimplantation embryonic development in mice [28]. Additionally, walnut-derived peptide TW-7 may enhance the development of parthenogenetic embryos obtained from vitrified MII oocytes by generating histone lactylation [29]. To evaluate the alterations and potential roles of lactylation in PCOS, LC–MS/MS was utilized to detect lactylation GC levels from patients with PCOS. Our findings revealed widespread lactylation dysregulation, characterized by an overall reduction in lactylation levels. Functional and pathway enrichment analyses demonstrated that DLPs were significantly enriched in processes, including the positive regulation of type I interferon production, neural crest cell migration, and bicarbonate transport. These results suggest that lactylation dysregulation in PCOS may contribute to disease pathogenesis by modulating immune responses, cell migration, and ion transport. Furthermore, DLPs were enriched in molecular functions, including R-SMAD binding and beta-catenin binding. The dysregulated activation of the TGF-β/Smad pathways has been implicated in the pathogenesis of fibrosis [30]. In recent years, the role of lactate, derived from metabolic reprogramming

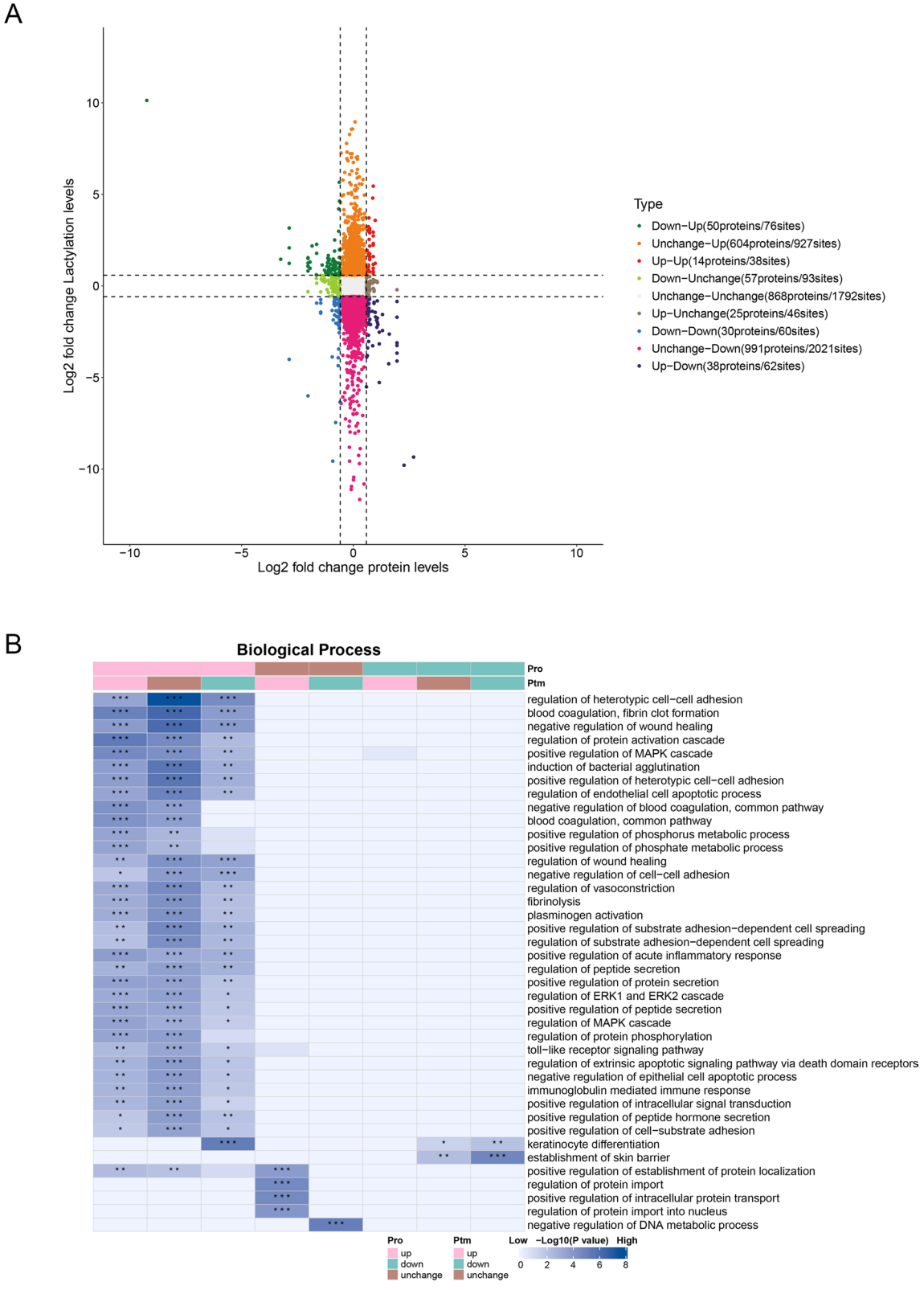

Fig. 7 Proteomics and modificationomics association analysis. **A** Distribution analysis of DEPs across the two omics datasets. **B** Clustering analysis of biological processes

(improved glycolysis), and its mediated histone lysine lactylation has become a research focus in fibrotic diseases, including pulmonary, hepatic, renal, and cutaneous fibrosis [31–38]. However, current studies face several challenges. First, most studies rely on animal models [38] and lack clinical validation [33]. Second, the competitive interplay between lactylation and other modifications (acetylation) [37] as well as inter-tissue differences, remains insufficiently explored. Many studies have investigated the role of the TGF-β/Smad signaling pathway in PCOS, especially in regulating granulosa cell apoptosis, fibrosis, and follicular development defects [39–45]. Consistent with this, we identified DLPs linked with R-SMAD and mapped them onto a PPI network. Using CytoHubba and MCODE algorithms, we identified crucial proteins, including SMAD3, SMAD2, CTNNB1, EP300, and JUN. These proteins were recognized as potential hub proteins by the CytoHubba algorithm (Fig. 6B) and further validated through MCODE clustering analysis (Fig. 6C). Proteomics analysis indicated that the expression levels of CTNNB1, EP300, SMAD3, and SMAD2 remained unchanged, whereas JUN expression was reduced in the PCOS group. Lactylation modifications play a pivotal role in regulating protein functions, even when protein abundance remains unchanged.

Epigenetic modifications of the transcriptional coactivators p300/CBP are closely linked to the regulatory mechanisms of the TGF-β/Smad signaling pathway in fibrotic conditions. Many studies have revealed the crucial role of p300 in modulating the TGF-β/Smad pathway through mechanisms that include acetylation and competitive binding. As a core coactivator in the TGF-β/Smad pathway, p300 exerts significant influence on fibrotic processes. Yuan and Varga [46] indicated that p300, through its HAT activity, reverses Smad3-mediated transcriptional suppression of matrix metalloproteinase-1, indicating that competitive binding between p300 and Smad regulates extracellular matrix degradation. Similarly, Kanamaru et al. [47] revealed in mouse mesangial cells that p300 interacts with Smad2/3 to promote α2(I) collagen expression, while Smad7 overexpression blocks this effect, highlighting the dual regulatory role of p300 in fibrosis. Cross-talk with other signaling pathways is also a significant consideration. Schiller et al. [48] demonstrated that cAMP activates CREB, which competes with p300 for binding, thereby preventing its interaction with Smad3 and antagonizing TGF-β-driven fibrotic gene expression (COL1A1, PAI-1). Chan et al. [49] further indicated that the prostacyclin receptor phosphorylates CREB, enabling its binding to p300 and blocking the formation of Smad transcriptional complexes, thereby suppressing myocardial fibrosis. Second, the tissue-specific roles of p300 in fibrosis are increasingly evident. In hepatic fibrosis, Zhang et al. [50] found that PPARβ/δ agonists reduce p300 levels and Smad3 phosphorylation through the AMPK/ERK pathway, thereby inhibiting the activation of hepatic stellate cells. In renal fibrosis, Tian et al. [51] reported that downregulation of p300 in aristolochic acid nephropathy correlates with reduced Smad7 expression, and that the imbalance between HDAC1 and p300 promotes renal interstitial fibrosis. In cardiac fibrosis, Bugyei–Twum et al. [52] reported that hyperglycemia activates the TGF-β pathway through p300-mediated Smad2 acetylation, while curcumin inhibits this process and enhances cardiac function. Finally, current studies have proposed several anti-fibrotic intervention strategies, including epigenetic regulation (HDAC1/p300 balance) and modulation of pathway cross-talk (cAMP/CREB). However, significant limitations remain: Most evidence is derived from cellular or animal models, with limited clinical translation, and the functional redundancy between p300 and CBP has not been fully resolved [48]. Moreover, HAT p300/EP300 is a core catalytic enzyme for lactylation [10]. Wei [29] reported that the walnut peptide TW-7 improves lactylation by upregulating LDHA/B and EP300, enhancing the embryonic development potential of vitrified oocytes, indicating the potential application of EP300 and lactylation in reproductive medicine.

Subcellular localization analysis of DEPs and DLPs demonstrated that most DEPs and DLPs are concentrated in the nucleus and cytoplasm, with 12.3% of DEPs and 7.4% of DLPs localized in the mitochondria. As mitochondria are the primary cellular organelles responsible for energy production, electron microscopy revealed mitochondrial damage in ovarian GCs from patients with PCOS. This finding suggests that lactylation modifications may be linked to mitochondrial function, underscoring the need for further investigation into their role in mitochondrial-related processes.

This study systematically characterized the lactylation modification profile in the GCs of patients with PCOS using 4D label-free proteomics, offering a new perspective on PCOS pathogenesis. Through interaction network analysis of DEPs and DLPs, several key proteins were identified, including SMAD2, SMAD3, CTNNB1, EP300, and JUN. Despite these advances, the study has some limitations. First, the relatively small sample size and the use of pooled samples limited the ability to fully capture the high heterogeneity of PCOS. Future research should aim to increase sample size and conduct stratified analyses based on different subtypes of PCOS (hyperandrogenemia and hyperinsulinemia) to improve the representativeness and generalizability of the results. Second, the current study primarily relies on static proteomics and lactylation modification analysis, failing to capture the dynamic alterations in lactylation under different physiological or pathological conditions. Future

research should integrate dynamic biological techniques, including real-time imaging and time-resolved mass spectrometry, to gain a deeper understanding of the roles of lactylation modifications and their dynamic regulation mechanisms in PCOS. Moreover, the identified key lactylated proteins have not yet been validated for their protein expression levels or lactylation modification levels. Future studies should employ lactylation-specific antibodies for validation. Besides, the specific mechanisms and functions of lactylation modification remain unclear, and subsequent studies should focus on site-specific lactylation of key proteins (SMAD2/3 and EP300) and their functional consequences, particularly regarding protein activity, stability, and subcellular localization. Another limitation of this study is the absence of validation using animal models. Future research should integrate animal models to elucidate the mechanisms of lactylation in PCOS and assess its clinical translational potential. Furthermore, the interactions between lactylation and other posttranslational modifications (acetylation and phosphorylation) and their regulatory effects on the TGF-β/Smad pathway warrant further exploration. Multi-omics approaches will be essential to dissect the interplay between lactylation and other modifications, thereby providing a more comprehensive understanding of their pathological roles in PCOS. Despite these limitations, this study offers valuable insights and highlights key directions for future research. First, it is essential to explore the role of lactylation modification in the TGF-β/Smad signaling pathway and the cross-talk between various modifications. For instance, it is crucial to investigate how lactylation modification dynamically regulates the key nodes of the TGF-β/Smad pathway and to study the synergistic or antagonistic effects between lactylation and acetylation modifications. Second, the roles of lactylation modifications in ovarian fibrosis and follicular development in PCOS require further clarification. Deepening the understanding of the specific effects of lactylation modifications on extracellular matrix remodeling, apoptosis, and follicular development in PCOS follicular cells could provide critical insights into the mechanisms underlying fibrosis and abnormal follicular development associated with PCOS. Furthermore, developing specific inhibitors or activators to regulate lactylation modifications and evaluating their effects on ovarian fibrosis and follicular development may offer new therapeutic strategies for PCOS. Moreover, we can explore the role of lactylation-modifying enzymes, including EP300, in regulating lactylation and their potential functions in follicle development and ovarian fibrosis. Furthermore, it is essential to evaluate the cross-regulation mechanisms between lactylation modifications and other signaling pathways (Wnt/β-catenin, PPARγ/NF-κB) and their regulatory effects on reproductive hormones (androgens and insulin). In summary, while this study has provided novel insights into the correlation between lactylation modifications and PCOS pathogenesis, additional research is needed to clarify the specific mechanisms and clinical translational potential. By addressing current limitations, employing multicenter, large-scale study designs, and integrating dynamic biological techniques and multi-omics approaches, future research can establish a stronger theoretical foundation for the precise treatment of PCOS.

Conclusions

In this study, quantitative protein expression profiles and lactylation-modified protein expression profiles of ovarian GCs in patients with PCOS were characterized, revealing differences in both overall protein abundance and lactylation-modified protein levels. These findings provide valuable insights into PCOS pathogenesis and offer potential clues for identifying therapeutic targets. However, the functional role of protein lactylation and its contribution to PCOS-related ovulatory dysfunction were not investigated in this study, representing an essential focus for future research.

Abbreviations

PCOS	Polycystic ovary syndrome
GCs	Granulosa cells
ICSI	Intracytoplasmic sperm injection
IVF-ET	In vitro fertilization-embryo transfer
LC–MS	Liquid chromatography–mass spectrometry
DEPs	Differentially expressed proteins
DLPs	Differentially lactylated proteins
TEM	Transmission electron microscopy
GO	Gene ontology
KEGG	Kyoto encyclopedia of genes and genomes
PPI	Protein–protein interaction
SMAD2	Mothers against decapentaplegic homolog 2
SMAD3	Mothers against decapentaplegic homolog 3
CTNNB1	Catenin beta-1
EP300	Histone acetyltransferase P300

Supplementary Information

The online version contains supplementary material available at https://doi.org/10.1186/s12014-025-09575-z.

Supplementary Material 1: Table S1. Proteomics of Ovarian GCs in Patients with PCOS.

Supplementary Material 2: Table S2. DEPs Identified in Proteomics.

Supplementary Material 3: Table S3. Lactylation-Modified Proteomics of Ovarian GCs in Patients with PCOS.

Supplementary Material 4: Table S4. Differentially Expressed Lactylated Proteins and Modification Sites Identified in Lactylation Proteomics.

Acknowledgements

We thank the patient for granting permission to publish this information.

Author contributions

LL, QG, and JY H: Investigation, Writing–original draft; YQ, KL L, YT, and YQ Z: Visualization, Data curation; YY L and YT L: Validation Analysis; XW N, YL H, and

HF Z: Project administration, Funding acquisition. All authors have read and agreed with the published version of the manuscript.

Funding
This work was supported by grants from the National Natural Science Foundation of China, Grant/Award Number: 82074479 and 82474567; Natural Science Foundation of Jiangsu Province，Grant/Award Number: BK20251964; Jiangsu Province Frontier Technology R&D Program Project，Grant/Award Number: BF2025618； Yixing Taodu Light Science and Technology Research Plan, Grant/Award Number: 2023SF12; Provincial Department of Education Postgraduate Innovation Project, Grant/Award Number: KYCX24_2245.

Data availability
All data generated or analysed during this study are included in this published article and its supplementary information files.

Declarations

Ethics approval and consent to participate
Clinical sample-related procedures received ethical clearance from the Jiangsu Province Hospital of Chinese Medicine's Ethics Committee (Approval No.2022NL-200-03), ensuring compliance with both institutional ethical standards and the Declaration of Helsinki principles. All patients signed informed consent.

Consent for publication
All of the authors have consented to publication of this research. All patients have consented to publication of this research.

Competing interests
The authors declare no competing interests.

Author details
[1]Department of Reproductive Medicine, Jiangsu Province Hospital of Chinese Medicine, Affiliated Hospital of Nanjing University of Chinese Medicine, Nanjing 210029, China
[2]Department of Gynaecology and Obstetric, Yixing Traditional Chinese Medicine Hospital, Yixing, Jiangsu, China

Received: 9 May 2025 / Accepted: 17 November 2025
Published online: 24 January 2026

References

1. Ajmal N, Khan SZ, Shaikh R. Polycystic ovary syndrome (PCOS) and genetic predisposition: a review article. Eur J Obstet Gynecol Reprod Biol X. 2019;3:100060.
2. Joshi A. PCOS stratification for precision diagnostics and treatment. Front Cell Dev Biol. 2024;12:1358755.
3. Choudhury JY, Elora N, Akther H, Chowdhury JJ, Bilkish US, Jaigyrder MKA. Evaluation and treatment strategies for infertile patients with diagnosed polycystic ovary syndrome (PCOS). Scholars International Journal of Obstetrics and Gynecology. 2024;7(07):289–95.
4. Zhu T, Cui J, Goodarzi MO. Polycystic ovary syndrome and risk of type 2 diabetes, coronary heart disease, and stroke. Diabetes. 2021;70(2):627–37.
5. Shrivastava S, Conigliaro RL. Polycystic ovarian syndrome. Med Clin North Am. 2023;107(2):227–34.
6. Jiang X, Yang Y, Li X, Li T, Yu T, Fu X. Lactylation: an innovative approach to disease control. Aging Dis. 2024;16(4):2130–50.
7. Vatier C, Christin-Maitre S. Epigenetic/circadian clocks and PCOS. Hum Reprod. 2024;39(6):1167–75.
8. Xie Y, Chen S, Guo Z, et al. Down-regulation of lon protease 1 lysine crotonylation aggravates mitochondrial dysfunction in polycystic ovary syndrome. MedComm. 2023;4(5):e396.
9. Wei H, Huo P, Liu S, Huang H, Zhang S. Posttranslational modifications in pathogenesis of PCOS. Front Endocrinol. 2022;13:1024320.
10. Zhang D, Tang Z, Huang H, et al. Metabolic regulation of gene expression by histone lactylation. Nature. 2019;574(7779):575–80.
11. Zhang C, Zhou L, Zhang M, et al. H3K18 lactylation potentiates immune escape of non-small cell lung cancer. Cancer Res. 2024;84(21):3589–601.
12. Pan RY, He L, Zhang J, et al. Positive feedback regulation of microglial glucose metabolism by histone H4 lysine 12 lactylation in Alzheimer's disease. Cell Metab. 2022;34(4):634-648.e6.
13. Zhu Y, Liu W, Luo Z, Xiao F, Sun B. New insights into the roles of lactylation in cancer. Front Pharmacol. 2024;15:1412672.
14. Yang D, Zheng H, Lu W, Tian X, Sun Y, Peng H. Histone lactylation is involved in mouse oocyte maturation and embryo development. Int J Mol Sci. 2024;25(9):4821.
15. Wu G, Pan Y, Chen M, et al. Lactylation drives hCG-triggered luteinization in hypoxic granulosa cells. Int J Biol Macromol. 2024;280:135580.
16. Zhang Y, Liu L, Yin TL, Yang J, Xiong CL. Follicular metabolic changes and effects on oocyte quality in polycystic ovary syndrome patients. Oncotarget. 2017;8(46):80472–80.
17. Sun L, Hu W, Liu Q, et al. Metabonomics reveals plasma metabolic changes and inflammatory marker in polycystic ovary syndrome patients. J Proteome Res. 2012;11(5):2937–46.
18. Zhao YK, Gao YN, Wang LC, Wang J, Wang GJ, Wu HL. Correlation between abnormal energy metabolism of ovarian granulosa cells and in vitro fertilization-embryo transfer outcomes in patients with polycystic ovary syndrome and obesity. J Ovarian Res. 2023;16(1):145.
19. Fontana J, Martínková S, Petr J, Žalmanová T, Trnka J. Metabolic cooperation in the ovarian follicle. Physiol Res. 2020;69(1):33–48.
20. Liu K, Wei H, Nong W, et al. Nampt/SIRT2/LDHA pathway-mediated lactate production regulates follicular dysplasia in polycystic ovary syndrome. Free Radic Biol Med. 2024;225:776–93.
21. Rotterdam ESHRE/ASRM-Sponsored PCOS consensus workshop group. Revised 2003 consensus on diagnostic criteria and long-term health risks related to polycystic ovary syndrome (PCOS). Hum Reprod. 2004;19(1):41–7.
22. Siddiqui S, Mateen S, Ahmad R, Moin S. A brief insight into the etiology, genetics, and immunology of polycystic ovarian syndrome (PCOS). J Assist Reprod Genet. 2022;39:2439–73.
23. Haddad-Filho H, Tosatti J, Vale FM, Gomes K, Reis F. Updates in diagnosing polycystic ovary syndrome-related infertility. Expert Rev Mol Diagn. 2023;23:123–32.
24. Zhang CH, Liu XY, Wang J. Essential role of granulosa cell glucose and lipid metabolism on oocytes and the potential metabolic imbalance in polycystic ovary syndrome. Int J Mol Sci. 2023;24(22):16247.
25. Liao B, Qi X, Yun C, Qiao J, Pang Y. Effects of androgen excess-related metabolic disturbances on granulosa cell function and follicular development. Front Endocrinol. 2022;13:815968.
26. Carmina E, Dreno B, Lucky WA, et al. Female adult acne and androgen excess: a report from the multidisciplinary androgen excess and PCOS committee. J Endocr Soc. 2022;6(3):bvac003.
27. Qian Y, Tong Y, Zeng Y, et al. Integrated lipid metabolomics and proteomics analysis reveal the pathogenesis of polycystic ovary syndrome. J Transl Med. 2024;22(1):364.
28. Yang W, Wang P, Cao P, et al. Hypoxic in vitro culture reduces histone lactylation and impairs pre-implantation embryonic development in mice. Epigenetics Chromatin. 2021;14(1):57.
29. Wei Y, Pan B, Qin J, et al. The walnut-derived peptide TW-7 improves mouse parthenogenetic embryo development of vitrified MII oocytes potentially by promoting histone lactylation. J Anim Sci Biotechnol. 2024;15(1):86.
30. Zaafan MA, Abdelhamid AM. Dasatinib ameliorates thioacetamide-induced liver fibrosis: modulation of miR-378 and miR-17 and their linked Wnt/β-catenin and TGF-β/smads pathways. J Enzyme Inhib Med Chem. 2022;37(1):118–24.
31. Li J, Zeng G, Zhang Z, et al. Urban airborne PM2.5 induces pulmonary fibrosis through triggering glycolysis and subsequent modification of histone lactylation in macrophages. Ecotoxicol Environ Saf. 2024;273:116162.
32. Cui H, Xie N, Banerjee S, et al. Lung myofibroblasts promote macrophage profibrotic activity through lactate-induced histone lactylation. Am J Respir Cell Mol Biol. 2021;64(1):115–25.
33. Zhou Y, Yan J, Huang H, et al. The m^6A reader IGF2BP2 regulates glycolytic metabolism and mediates histone lactylation to enhance hepatic stellate cell activation and liver fibrosis. Cell Death Dis. 2024;15(3):189.
34. Wang Y, Li H, Jiang S, et al. The glycolytic enzyme PFKFB3 drives kidney fibrosis through promoting histone lactylation-mediated NF-κB family activation. Kidney Int. 2024;106(2):226–40.
35. Zhang X, Chen J, Lin R, et al. Lactate drives epithelial-mesenchymal transition in diabetic kidney disease via the H3K14la/KLF5 pathway. Redox Biol. 2024;75:103246.

36. Wang P, Xie D, Xiao T, et al. H3K18 lactylation promotes the progression of arsenite-related idiopathic pulmonary fibrosis via YTHDF1/m^{6}A/NREP. J Hazard Mater. 2024;461:132582.
37. Rho H, Terry AR, Chronis C, Hay N. Hexokinase 2-mediated gene expression via histone lactylation is required for hepatic stellate cell activation and liver fibrosis. Cell Metab. 2023;35(8):1406-1423.e8.
38. Wu S, Li J, Zhan Y. H3K18 lactylation accelerates liver fibrosis progression through facilitating SOX9 transcription. Exp Cell Res. 2024;440(2):114135.
39. Shen H, Wang Y. Activation of TGF-β1/Smad3 signaling pathway inhibits the development of ovarian follicle in polycystic ovary syndrome by promoting apoptosis of granulosa cells. J Cell Physiol. 2019;234(7):11976–85.
40. Yu M, Liu J. Microrna-30d-5p promotes ovarian granulosa cell apoptosis by targeting Smad2. Exp Ther Med. 2020;19(1):53–60.
41. Chen L, Yan X, Lian Y, et al. Dingkun pill-mediated TGF-β1/Smad2 pathway effects on granulosa cell proliferation and apoptosis. Mol Biotechnol. 2025. https://doi.org/10.1007/s12033-025-01439-z.
42. Wang D, Wang W, Liang Q, et al. DHEA-induced ovarian hyperfibrosis is mediated by TGF-β signaling pathway. J Ovarian Res. 2018;11(1):6.
43. Zhou Y, Lan H, Dong Z, Cao W, Zeng Z, Song JL. Dietary proanthocyanidins alleviated ovarian fibrosis in letrozole-induced polycystic ovary syndrome in rats. J Food Biochem. 2021;45(5):e13723.
44. Zhou YY, He CH, Lan H, Dong ZW, Wu YQ, Song JL. Rhamnocitrin decreases fibrosis of ovarian granulosa cells by regulating the activation of the PPARγ/NF-κB/TGF-β1/Smad2/3 signaling pathway mediated by Wisp2. Ann Transl Med. 2022;10(14):789.
45. Ghorbani M, Sanoee Farimani M, Khodadadi I, Mohagheghi S, Amiri I, Tayebinia H. The regulatory roles of Smad2/3 protein and SMURF2 gene expression in granulosa cells of germinal vesicle and metaphase II oocytes in polycystic ovarian syndrome: a case-control study. International Journal of Reproductive BioMedicine (IJRM). 2024;22(6):441–50.
46. Yuan W, Varga J. Transforming growth factor-beta repression of matrix metalloproteinase-1 in dermal fibroblasts involves Smad3. J Biol Chem. 2001;276(42):38502–10.
47. Kanamaru Y, Nakao A, Tanaka Y, et al. Involvement of p300 in TGF-beta/smad-pathway-mediated alpha2(I) collagen expression in mouse mesangial cells. Nephron Exp Nephrol. 2003;95(1):e36–42.
48. Schiller M, Dennler S, Anderegg U, et al. Increased cAMP levels modulate transforming growth factor-beta/smad-induced expression of extracellular matrix components and other key fibroblast effector functions. J Biol Chem. 2010;285(1):409–21.
49. Chan EC, Dusting GJ, Guo N, et al. Prostacyclin receptor suppresses cardiac fibrosis: role of CREB phosphorylation. J Mol Cell Cardiol. 2010;49(2):176–85.
50. Zhang M, Barroso E, Peña L, et al. PPARβ/δ attenuates hepatic fibrosis by reducing SMAD3 phosphorylation and p300 levels via AMPK in hepatic stellate cells. Biomed Pharmacother. 2024;179:117303.
51. Tian Y, Yang Y, Gao L, et al. Expression of histone deacetylase-1 and p300 in aristolochic acid nephropathy models. Toxicol Mech Methods. 2014;24(6):377–84.
52. Bugyei-Twum A, Advani A, Advani SL, et al. High glucose induces smad activation via the transcriptional coregulator p300 and contributes to cardiac fibrosis and hypertrophy. Cardiovasc Diabetol. 2014;13:89.

Publisher's Note